Dynamics of bubble breakup at a T junction

Yutao Lu, Taotao Fu, Chunying Zhu, Youguang Ma, Huai-Zhi Li

Dynamics of bubble breakup at a T junction

Yutao Lu,[1] Taotao Fu,[1,*] Chunying Zhu,[1] Youguang Ma,[1,†] and Huai Z. Li[2]

[1]*State Key Laboratory of Chemical Engineering, Collaborative Innovation Center of Chemical Science and Engineering (Tianjin), School of Chemical Engineering and Technology, Tianjin University, Tianjin 300072, China*

[2]*Laboratory of Reactions and Process Engineering, University of Lorraine, CNRS, 1, rue Grandville, BP 20451, 54001 Nancy cedex, France*

(Received 29 January 2015; revised manuscript received 21 December 2015; published 22 February 2016)

The gas-liquid interfacial dynamics of bubble breakup in a T junction was investigated. Four regimes were observed for a bubble passing through the T junction. It was identified by the stop flow that a critical width of the bubble neck existed: if the minimum width of the bubble neck was less than the critical value, the breakup was irreversible and fast; while if the minimum width of the bubble neck was larger than the critical value, the breakup was reversible and slow. The fast breakup was driven by the surface tension and liquid inertia and is independent of the operating conditions. The minimum width of the bubble neck could be scaled with the remaining time as a power law with an exponent of 0.22 in the beginning and of 0.5 approaching the final fast pinch-off. The slow breakup was driven by the continuous phase and the gas-liquid interface was in the equilibrium stage. Before the appearance of the tunnel, the width of the depression region could be scaled with the time as a power law with an exponent of 0.75; while after that, the width of the depression was a logarithmic function with the time.

DOI: 10.1103/PhysRevE.93.022802

I. INTRODUCTION

In recent years, microfluidics was applied in many domains, such as chemical engineering, materials engineering, and the analysis of chemicals [1–4]. Gas-liquid two-phase flow in microchannels was the basis for the applications of microfluidics technique [5–8]. Bubbles are always encountered in gas-liquid two-phase flow in microchannels and it is of importance to control the size of bubbles [7,9]. T junction is the most popular employed geometry for the microfluidic device to passively tailor the bubble size and is one of the most popular geometries for the parallelization of microchannels for the scale-up of microfluidic devices [10–12]. Therefore, it is necessary to study the bubble breakup in T junctions.

The T junction is first employed to tailor droplets into smaller ones, with the characteristic parameters defined in Fig. 1(a) [9,12,13]. Thus, we summarize the droplet breakup at T junctions before reviewing the bubble breakup at T junctions. Link *et al.* [9] pioneered to study the breakup and distribution of droplets in T junctions. It was identified that the droplet will breakup into smaller ones under the classical Rayleigh-Plateau instability, if the length of the droplet is larger than its circumference at maximum extension. Therefore, whether a droplet will breakup or not depends on the capillary number and the original length of the droplet. Later on, Leshansky *et al.* [14] found a two-dimensional mechanism for the partly droplet breakup in a symmetric T junction that is driven by the increased upstream pressure due to lubrication flow in a thin film in the narrow gap between the droplet and the channel wall at moderate and low capillary numbers. In the partly obstructed breakup of a droplet, the droplet extends under the confinement of the wall and finally breaks up into smaller ones driven by an increased upstream pressure due to lubrication flow in a thin film between the droplet and the channel wall at high surface tension (low capillary number). Leshansky *et al.* [14] described successfully the liquid-liquid interface shape for a breaking droplet using a geometric construction with lubrication analysis in the narrow tunnel between the droplet and the channel wall at moderate capillary numbers. Furthermore, the dependence of the critical droplet's extension L_c and the maximum width of the tunnel w_{tmax} on the capillary number Ca were derived, respectively, as $L_c/w \approx 1.3\mathrm{Ca}^{-0.21}$ and $w_{\mathrm{tmax}}/w \approx \mathrm{Ca}^{2/5}$, where w is the channel width as shown in Fig. 1(a). Leshansky *et al.* [14] also found a critical width δ_c/w of the deformed droplet to breakup, which is $1/2$ as gathered in Table I. Jullien *et al.* [15] identified the theoretical results established by Leshansky *et al.* [14] for droplet breakup in a three-dimensional device and found a critical value of $\delta_c/w = 0.3$ for the width of the deformed droplet to breakup (Table I). By using the same methodology, Leshansky *et al.* [16] also investigated the breakup of a long droplet with permanent obstruction in a T junction. It was shown that the variation of the length of the depression region L_{d} with the dimensionless time Ut/w (t is the time, and U is the mean inlet velocity) can be scaled by a power-law relationship as $L_{\mathrm{d}}/w \propto (Ut/w)^{4/7}$, and the width of the depression region w_{d} and the width of the minimum neck of the droplet δ can be scaled with the dimensionless time, respectively, as $w_{\mathrm{d}}/w \propto (Ut/w)^{3/7}$, $\delta/w \propto 1-(Ut/w)^{3/7}$. Recently, Hoang *et al.* [17] performed a numerical study on the breakup of a droplet in T junction and found a critical width δ_{c} of the droplet neck that determines the breaking rate of the droplet by using a stop-flow simulation: if the minimum width of the droplet neck was less than the critical value, the breakup was fast and autonomous; while if the minimum width of the neck was larger than the critical value, the breakup was slow. The slow breakup of a droplet was driven by the externally applied flow, during which the droplet deformation was quasisteady. The fast breakup of a droplet was analogous to the three-dimensional end-pinching mechanism for an unconfined droplet, which was driven by the surface tension and was independent of the externally applied flow. The critical width of the droplet neck was determined at the time when the curvature at the droplet neck was equal to the curvature everywhere else in

*ttfu@tju.edu.cn
†ygma@tju.edu.cn

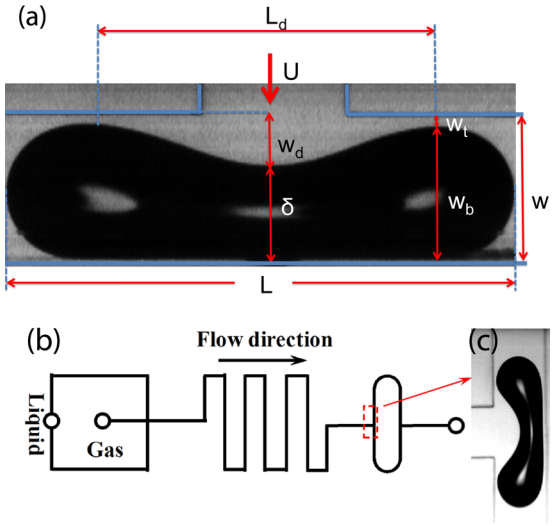

FIG. 1. (a) A scheme for the definition of geometrical parameters for bubble (droplet) breakup at a T junction. U is the mean inlet velocity, δ the minimum width of the bubble neck, w the channel width, $L_{\rm d}$ the length of depression region, w_d the width of depression region, L the length of the breaking bubble, $w_{\rm b}$ the maximum width of the bubble tip, and $w_{\rm t}$ the width of the tunnel between the bubble tip and the channel wall. (b) Sketch of the microfluidic device. Bubbles are generated at a flow-focusing junction and move toward a curved channel to pass through a loop with a T-junction divergence. (c) A breaking bubble at the T-junction divergence.

the midplane of the channel, and depended strongly on the height-to-width ratio h of the channel as $\delta_{\rm c} = \frac{h}{h+1}$ (Table I). But, contrary to the droplet breakup in unconfined flows, the critical width of the droplet neck hardly depended on the capillary number and the viscosity contrast between the two fluids. In addition, in the fast breakup stage, the minimum width of the droplet neck was proportional to the time as $\delta \propto t$.

For bubble breakup at T junctions, the breakup dynamics of a bubble depends on the relative length scale ratio of the bubble to the channel and the flowing fluids in microchannels [18,19]. For the permanently obstructed breakup of a long bubble, the thinning of the bubble is predominated by the augmented pressure in the obstructed liquid around the bubble, which depends on the gas and liquid flow rates [18]. For the partly obstructed breakup of a medium-sized bubble [18], a critical width of the bubble neck δ_c was observed. When $\delta_c/w > 0.625$, the breakup is slow; and if $\delta_c/w < 0.625$, the breakup is fast (Table I). Fu *et al.* [18] insisted that the distinct divergence of the breakup rate of a bubble was caused by the reduction of the pressure in the depression region with the leaking of the continuous phase through the tunnel. For bubble breakup with permanent tunnels, the scaling of the minimum width of the bubble neck in the final breakup can be expressed as $\delta \propto \tau^{0.33}$. Recently, Wang *et al.* [20] studied systematically bubble breakup with permanent obstruction in an asymmetric T junction and found that the breakup process of a long bubble in the T junction could be divided into the squeezing stage, the transition stage, and the pinch-off stage. In the squeezing stage, the bubble thins nonlinearly with time. In the transition stage, the bubble thins linearly with time. In the pinch-off stage, the minimum width of the bubble neck with the remaining time could be scaled as a power-law relationship. During the whole breakup process, the mean velocity of the flowing fluid is a key factor influencing the thinning of the bubble neck, and its augment could promote the thinning of the bubble. Wang *et al.* [20] found that the dimensionless critical neck width δ_c/w of the breaking bubble for the onset of the rapid collapse stage is within $0.25 \sim 0.4$, depending on the capillary number and the liquid viscosity (Table I). Wang *et al.* [21] observed recently that the critical neck width of the breaking bubble

TABLE I. Critical width of the neck for the breaking droplet or bubble.

Critical width of the neck δ_c/w	Droplet or bubble	Conditions	Channel geometry	Breakup type	Note	Reference
1/2	Droplet	$Ca^{1/5} \ll 1$	Two-dimensional simulation, symmetric T junction	Partly obstructed	Onset of breakup	Leshansky *et al.* (2009) [14]
0.3	Droplet	$3 \leqslant l/w \leqslant 6$	Rectangular, symmetric T junction	Partly obstructed	Onset of breakup	Jullien *et al.* (2009) [15]
$\frac{h}{h+1}$	Droplet	$0.33 < h < 1, l/w \geqslant 2.80$	Rectangular, symmetric T junction	Obstructed and nonobstructed	Onset of the rapid collapse	Hoang *et al.* (2013) [17]
0.625	Bubble	Liquid viscosity $\in$ [2.32,10.18]mPas; $0.0046 \leqslant$ Ca $\leqslant 0.017$; $2.43 \leqslant l/w \leqslant 2.93$	Square, symmetric T junction	Partly obstructed	Onset of the rapid collapse	Fu *et al.* (2011) [18]
$0.25 \sim 0.4$	Bubble	Liquid viscosity $\in$ [0.92,9.56]mPas; $0.002 \leqslant$ Ca $\leqslant 0.3$; $2.5 \leqslant l/w \leqslant 7$	Square, asymmetric T junction	Permanent obstruction	Onset of the rapid collapse	Wang *et al.* (2015) [20]
0.14–0.22	Bubble	$0.0004 \leqslant$ Ca $\leqslant 0.006$; $2.74 \leqslant l/w \leqslant 4$	Rectangular, symmetric T junction	Partly obstructed	Onset of the rapid collapse	Wang *et al.* (2015) [21]
0.5–0.6	Bubble	Ca $\in$ [0.003877,0.0155]	Square, symmetric T junction	Obstructed and nonobstructed	Onset of the rapid collapse	Figs. 8, 11, and 14 in the present work

TABLE II. Dynamics of bubble breakup in a T junction.

		Bubble neck δ, for fast breakup				Tunnel	
	Bubble neck δ, for slow breakup	the rearrangement stage	the fast pinchoff	Bubble length L	Depression regime w_d	the slow breakup	the fast breakup
Regime A	$k_n < k_t$; The collapse rate of the bubble neck decreases gradually	$k_n > k_t$; $\delta \propto \tau^{0.22\pm0.02}$	$k_n > k_t$; $\delta \propto \tau^{0.50\pm0.02}$	L increases at a certain fixed rate during the whole	For the slow-breakup stage $w_d/w \propto (\tau_{do} - \tau)^{0.75}$	—	—
Regime B	the evolution of δ differs before and after the appearance of the tunnel	$\delta \propto \tau^{0.22\pm0.02}$	$\delta \propto \tau^{0.50\pm0.02}$	In the slow breakup, L increases linearly with different slopes before and after the appearance of the tunnel. In the fast breakup, L increases nonlinearly	Before the appearance of the tunnel, $w_d/w \propto (\tau_{do} - \tau)^{0.75}$; after the appearance of the tunnel, $w_d/w \propto a\ln(\tau_{do} - \tau) + b$	$w_t/w \propto (\tau_{to} - \tau)^{0.75}$	$w_t/w = 0.0885\tau^{0.21}$
Regime C	the tendency in regime C deviates from that in the regime B	$\delta \propto \tau^{0.22\pm0.02}$;	$\delta \propto \tau^{0.50\pm0.02}$	L increases linearly in the slow breakup stage, and increases nonlinearly in the fast breakup stage	In the slow breakup stage, $w_d/w = 0.1676 \ln(\tau_{do} - \tau) + 0.2819$	$w_t/w \propto (\tau_{to} - \tau)^{0.75}$	$w_t/w \propto \tau^{0.12}$
Regime D	—	—	—	—	—	—	—

for the onset of the rapid collapse stage in a rectangular symmetric T junction is related to the capillary number and the length of the original bubble l as gathered in Table I.

In comparison with droplet breakup in T junctions, the dynamics and mechanism of bubble breakup in T junctions have not been fully understood [22]. This work presents detailed information on the evolution of the gas-liquid interface during bubble breakup in a flowing fluid under confinement in a T junction. Four regimes are observed for bubbles flowing through the T junction, depending on whether the bubble breakup or not, and whether a tunnel between the bubble and channel wall opens or not. A critical minimum width of the bubble neck is found to be existed to distinguish the fast and slow breakup stages of bubbles at T junctions, which is within 0.5–0.6. The scaling laws for the interfacial dynamics during bubble breakup in three various types in the T junction are also provided, as shown in Table II. Moreover, before the appearance of the tunnel, the dynamics of the depression region is studied in detail.

II. EXPERIMENTAL PROCEDURES

As shown in Fig. 1, a square cross-sectional microchannel of 400 × 400 μm was employed in the experiment. The width of the channel w is 400 μm. The channel was fabricated in a polymethyl methacrylate (PMMA) plate by precision milling, and then sealed with another PMMA plate by screws. The gas and liquid flow rates (Q_g and Q_l, respectively) were controlled, respectively, by syringe pumps (PHD 2000, Harvard Apparatus, America). The accurate performance of the pumps makes it feasible to control stop-flow and makes it possible to control the flow conditions of bubbles. The dispersed phase N_2 was infused to the main channel, and the continuous phase to the two lateral channels at a flow-focusing junction [Fig. 1(b)]. Bubbles were formed in the flow-focusing junction and then moved downstream toward a T-junction divergence in a loop as shown in Fig. 1(c). To avoid the reciprocal effect of bubble breakup at the T junction and bubble formation at the flow-focusing region, a long and curved channel was designed between the formation section and the breakup sections for bubbles as shown in Fig. 1(b). The images were captured when the flow was steady for each flow condition after a waiting time, which depends on the operating conditions. The scene of bubble breakup at the T junction was magnified by a microscope (ECLIPSE Ti-U, Nikon, Japan) and was recorded by a high-speed digital camera (MotionPro Y5, IDT, USA). The highest frequency of the camera was 100 kfps (kilo frame per second), with a shortest exposure time of 1 μs. In this work, 10 and 2 kfps were used for various experimental conditions. The spatial resolution of the images was up to 2 μm/pixel. The images captured by the camera were then processed with a homemade Matlab program to obtain the characteristic parameters for the breaking bubbles, with an error of ± 2 μm (1 pixel) for the lengthscale. Nitrogen and turpentine oil were used as the dispersed and the continuous phases, respectively. The turpentine oil, with viscosity $\mu = 1.34$ mPa s, density $\rho = 867\,\mathrm{kg/m^3}$, surface tension $\sigma = 24$ mN/m, and contact angle $\theta = 15^\circ$ on a flat PMMA, has a good wetting property to the channel walls. The capillary number Ca

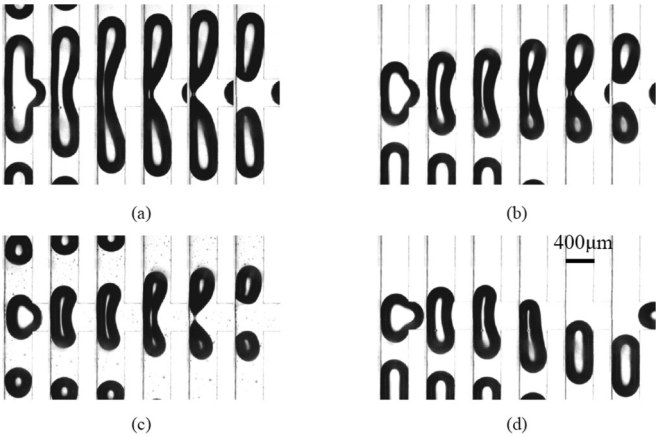

FIG. 2. Four regimes observed for bubbles move across the T divergence. (a) Regime A, breakup of long bubbles with permanent obstruction; (b) regime B, breakup of medium-sized bubbles with partly obstruction; (c) regime C, breakup of short bubbles with permanent gaps; (d) regime D, nonbreakup of bubbles.

(Ca $= U\mu/\sigma$) ranged from 0.003877 to 0.01551, where U is the mean velocity of the gas-liquid two-phase flow and $U = (Q_g + Q_l)/w^2$.

III. RESULTS AND DISCUSSION

A. Flow regimes for bubbles moving though the T junction

There are four regimes when a bubble moves through the T-junction divergence, which depends on whether the bubble breaks up or not, or whether a tunnel exists or not between the bubble and the channel wall [15,18]. The regime for the breakup of a long bubble is named A as shown in Fig. 2(a), during which the bubble is confined by the channel walls and no tunnel appears between them. When a bubble moves through the T junction, the bubble is driven to the two arms and the interface is concave under the squeezing of the continuous phase until the final pinch-off of the gas-liquid interface. During this process, the tips of the bubble keep a steady shape and the variation of the gas-liquid interface only occurs on the neck of the bubble. The regime for the breakup of a medium-sized bubble is named B as shown in Fig. 2(b). During this process, the bubble breaks up with obstruction after entering the junction, during which the bubble is confined by the channel walls and no tunnels appear. And in a certain period, a tunnel between the bubble and the channel wall on the feeding channel side appears, through which the continuous phase can pass. The regime for the breakup of a short bubble is named C as shown in Fig. 2(c). The tips of the bubble detach the channel wall on the feeding channel side as soon as the bubble enters the T junction, and the tunnel between the bubble tip and the channel wall always exists during the entire breakup process of the bubble. It is noteworthy that the existence of the obstruction period during bubble breakup in regime B makes it different from regime C, which has no such period. Another regime named D is the nonbreakup of bubbles as shown in Fig. 2(d). The bubble moves across the T junction without breakup.

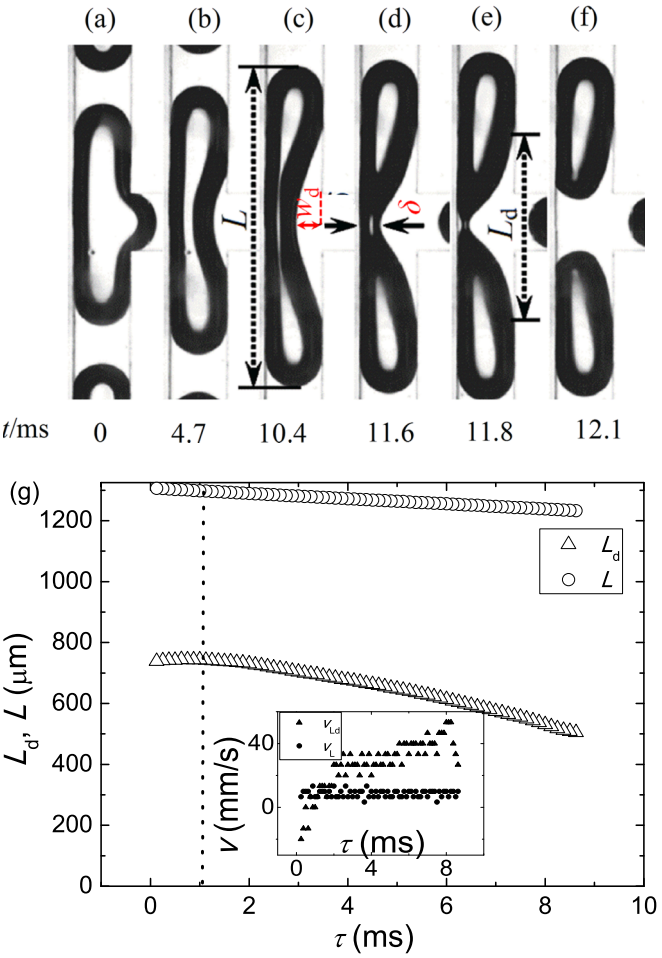

FIG. 3. (a)–(f) Bubble breakup in regime A. (g) Evolution of the length of depression L_d and length of the bubble L with the remaining time τ. The inset illustrates the evolution rate of the bubble and the depression region in the arms' direction with the remaining time, with the definition of $v_{Ld}[v_{Ld}=\Delta L_d/(-\Delta\tau)]$ and $v_L[v_L=\Delta L/(-\Delta\tau)]$, respectively. $Q_l = 20\,\text{mL/h}, Q_g = 30\,\text{mL/h}$. The capillary number Ca $= 0.004847$.

B. Mechanism and dynamics of bubble breakup at the T-junction in flow regime A

A typical process for the breakup of a long bubble at the T junction is shown in Figs. 3(a)–3(f). When the bubble enters the T junction to block it, a depression region is formed at the junction. A curved gas-liquid interface is formed at the junction, when the continuous phase invades into the divergence. Due to the obstruction for the liquid, the pressure in the depression region increases gradually, and the width of the depression region augments to thin the bubble neck. When the bubble neck detaches from the subjacent wall, the bubble breaks up rapidly into two small bubbles. Figure 3(g) illustrates the evolution of the length L_d of the depression region with the remaining time τ. During the slow breakup, the depression region extends under the squeezing of the continuous phase so that the length of the depression region L_d increases gradually to reach a maximum value at the end of the slow breakup as shown in the inset of Fig. 3(g). During the fast breakup, the length of the depression region

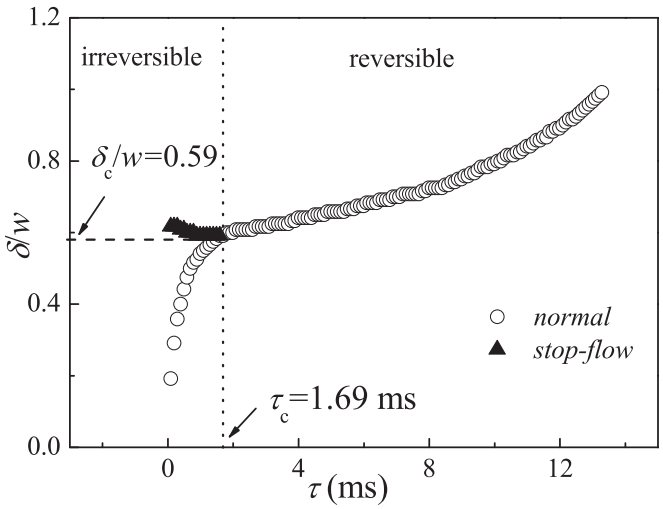

FIG. 4. Evolution of the minimum width δ of the bubble neck with the remaining time τ before the final pinchoff for bubble breakup in regime A. δ_c is the critical minimum width of the breaking bubble, identifying the slow- and rapid-breakup stages, which occurs at the critical remaining time $\tau_c = 1.69$ ms. The vertical dotted line characterizes the critical remaining time, and the horizontal dashed line represents the critical width of the breaking bubble. The liquid flow rate $Q_l = 10$ mL/h, the gas flow rate $Q_g = 30$ mL/h. The capillary number Ca = 0.003877.

L_d decreases gradually. Furthermore, the squeezing of the liquid phase fades, and the reversed liquid flows toward the bubble neck from the bubble tip through the gap between the bubble and the channel wall [23], due to the fast breakup of the bubble. Therefore, the depression region shrinks toward the bubble neck to reduce the length of depression region during fast breakup of the bubble, due to the mass conservation of the breaking bubble [18]. In addition, as shown in the inset of Fig. 3(g), the length of the bubble increases at a certain fixed rate during the whole breakup and the rate approximates the half of the original one, signifying that the flux of the reversed flow is small during the breakup of the long bubble at the T junction.

It is found that the thinning of the bubble neck experiences a slow-breakup stage and a fast-breakup stage by examining the evolution of the minimum width δ of the bubble neck with the remaining time τ before the final pinch-off for bubble breakup in regime A as shown in Fig. 4. The rate of the bubble breakup decreases first and increases when the minimum width of the bubble neck is less than a critical value of $\delta_c/w = 0.59$, where δ_c is the critical minimum neck width for the breaking bubble between the slow- and fast-breakup stages. When the minimum width of the neck is larger than the critical value δ_c, the breakup is driven by the continuous phase and this stage is the slow-breakup stage; and when the minimum width of the neck is less than the critical value δ_c, the breakup is driven by the surface tension and this stage is the rapid-breakup stage. This phenomenon is similar to the observation of several recent publications as listed in Table I [14,15,17,18,20,21]. To explore the role of the continuous phase on the bubble breakup under the confinement at the microfluidic T junction, the "stop-flow" method is employed [17,24], realized by stopping the pumps at a moment during the bubble-breaking process. As shown in Fig. 4, the concave neck of the bubble restore to the original state during the slow-breakup stage; and the breakup continues during the rapid breakup stage. It is identified that the slow breakup is reversible and the fast breakup is irreversible. This phenomenon is similar to the simulation results in Hoang *et al.* [17] and other publications [14,15,18,20,21] as summarized in Table I. Garstecki *et al.* [25] insisted that the gas-liquid interface is on the equilibrium state with the combined action of liquid squeezing and the surface tension in a linear breakup stage for bubble formation in a flow-focusing junction. Similar phenomena were observed for the axisymmetric breakup of the gaseous thread during bubble formation in flow-focusing devices [26–28]: the minimum width of the gaseous thread thins with varying speed for the slow- and fast-breakup stages, due to the different physical mechanisms at play for bubble pinchoff. In the slow-breakup stage, the neck of the gaseous thread collapses with a scaling law of 1/3, which can be explained by the filling effect of the continuous phase toward the collapsing thread [27,28]. In the fast-breakup stage, the collapse can be characterized by a scaling exponent of 2/5 [27] or 1/2 [28], depending on the geometry of the flow-focusing devices, demonstrating a liquid inertia-driven mechanism and the always important surface-tension effects. In the present study, the similar qualitative varying speed for the asymmetric breakup of the bubbles in the T junction suggests similar physical mechanisms at play, with some modifications by the effects of the confinement of the microchannel on the breaking bubbles in the two geometries.

The role of the surface tension in the bubble breakup is determined by the curvature of the gas-liquid interface. According to previous conclusions of Hoang *et al.* [17], Lu *et al.* [28], and van Steijn *et al.* [23], whether a bubble breakup spontaneously or not is determined by the relative value of the curvature of the bubble neck to that of other positions for the gas-liquid interface: the bubble neck will breakup spontaneously predominated by the surface tension, when the curvature of the bubble neck is larger than that of other positions for the bubble. The evolution of the curvature of the bubble neck k_n and tip k_t with the remaining time τ is illustrated in Fig. 5. In the slow-breakup stage, the curvature of the bubble neck is less than that of the tip. In the fast-breakup stage, the curvature of the bubble neck is larger than that of the tip, signifying that the fast breakup is driven by the surface tension [29]. It should be pointed out that this fast-breakup stage is also driven by the inertia of the liquid as shown in Ref. [27], as the neck becomes less slender during the pinchoff. It should be also noted that, according to Leshansky *et al.* [16] and Fu *et al.* [18], the breakup of bubble under confinement is predominated by the relative value of the length scale of the gas-liquid interface to the channel, which is related to the flow regimes for bubble breakup in microchannels.

To further explore the mechanism for bubble breakup at the T junction, the evolution and scaling law of the minimum width of the bubble neck with the remaining time is illustrated in detail in Fig. 6. The thinning of the neck of the bubble experience an initiating stage, a liquid squeezing slow-breakup stage, and a fast-breakup stage. In the fast-breakup stage, the bubble thins at two varied speeds. At the beginning, the minimum width of the bubble neck thins with the remaining time

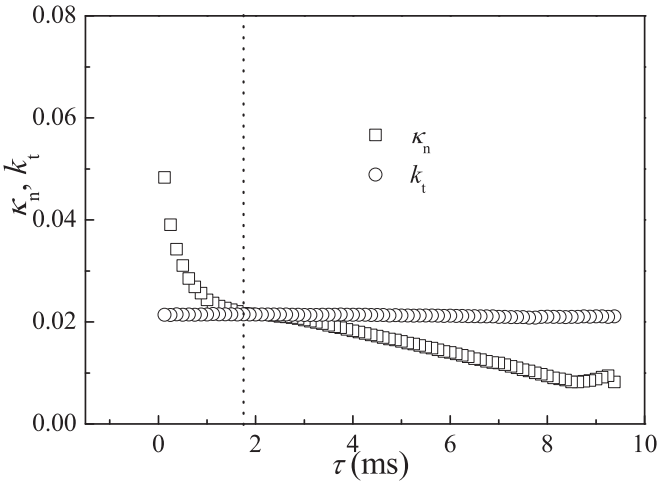

FIG. 5. Evolution of curvature of bubble neck k_n and tip k_t with the remaining time τ. $Q_l = 10$ mL/h, $Q_g = 30$ mL/h. The vertical dotted line characterizes the critical remaining time. The capillary number Ca = 0.003877.

as a power-law with an exponent of 0.22 in the rearrangement stage, followed by a 0.49 scaling law free pinchoff stage. There is obvious diversity between the slow-breakup stage and the fast-breakup stage, and the critical width of the neck of the breakup bubble δ_c/w is found to be 0.5 in Fig. 6. Therefore, we investigate the law of breakup during the slow stage and the fast stage, respectively. As shown in Fig. 6, the collapse rate of the bubble neck decreases gradually in the slow-breakup stage due to the amplification of the depression region, which can be characterized by the length L_d and width w_d of the depression region as shown in Figs. 3(c) and 3(e). During the breakup of

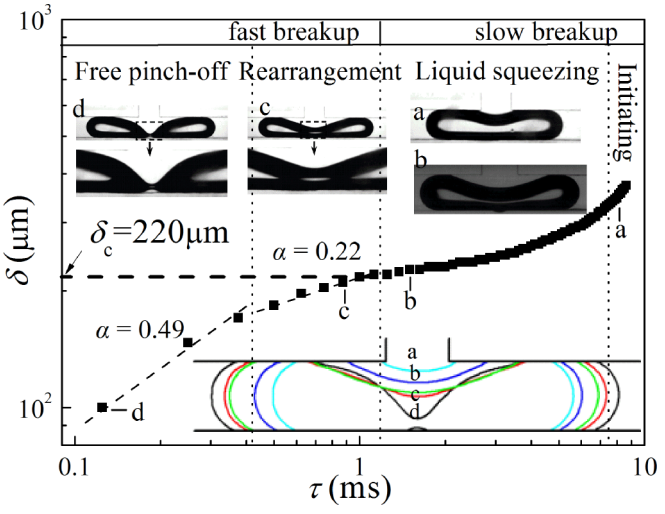

FIG. 6. Evolution of the minimum width of bubble neck with the remaining time in regime A. The insets (a)–(d) were the optical micrographs of the gas-liquid interface during the breakup of the bubble. The subjacent inset gives the evolution of bubble profile during its breakup. $Q_l = 20$ mL/h, $Q_g = 30$ mL/h. The capillary number Ca = 0.004847. The vertical dotted lines differentiate the boundaries between adjacent stages. The horizontal dashed line represents the critical minimum width of the breaking bubble δ_c.

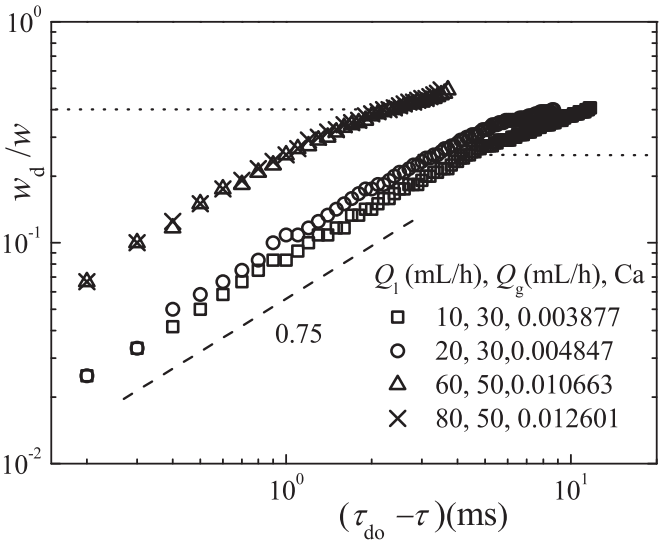

FIG. 7. Evolution of the width of depression region w_d/w with the time $(\tau_{do} - \tau)$ during the slow breakup of bubbles in regime A. τ_{do} is the remaining time before the final pinchoff when the depression region starts to form. The horizontal lines differentiate the slow- and fast-breakup stages.

the bubble, the variation of the depression region suggests that the length L_d and width w_d of the depression region changes with time [16]. During the slow collapse process, the variation of the width of the depression region w_d with the time $(\tau_{do} - \tau)$ can be scaled by a power-law relationship as $w_d/w \propto (\tau_{do} - \tau)^{0.75}$, as shown in Fig. 7, where τ_{do} is the remaining time before the final pinchoff when the depression region starts to form. The scaling law is inconsistent with the result of Leshansky *et al.* [16], in which the 3/7 law is obtained by the 2D lubrication theory. However, the cross-section of the channel is square in this study and there is strong deformation in the depth direction. Therefore, the 2D lubrication theory

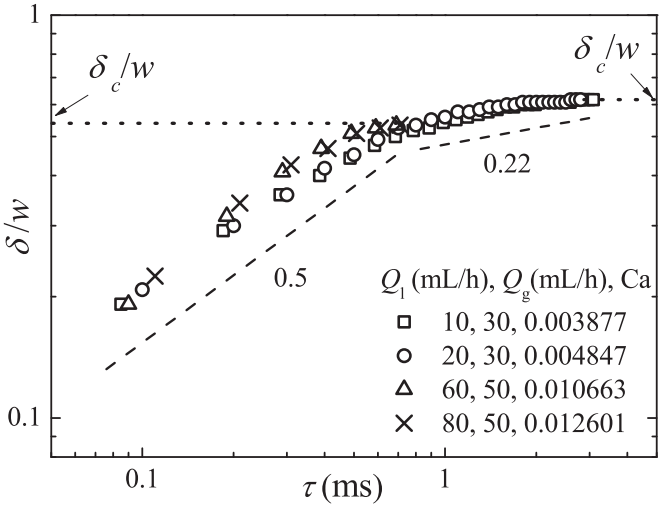

FIG. 8. Evolution of the minimum width of the bubble neck δ with the remaining time τ during the fast breakup in regime A. The horizontal dotted lines show the critical minimum width of the breaking bubble δ_c.

is invalid for this study. In addition, the exponent decreases rapidly approaching the end of the slow breakup, implying that there is strong deformation of the bubble, making the thinning of the bubble experiences the rearrangement stage.

In the fast-breakup stage, the evolution of the minimum width of the neck with the remaining time follows a power law function and the exponent increases gradually during the breakup, as shown in Fig. 8. The exponent is about 0.22 on the beginning of the fast breakup (the rearrangement stage) and is 0.5 approaching to the final pinchoff (the free pinchoff stage). Furthermore, the breakup rate is independent of the liquid flow rate. This phenomenon is similar to the breakup dynamics for bubble formation in a flow-focusing device as discussed previously [27,28]. van Hoeve *et al.* [27] observed two stages for the axisymmetric collapse of the gaseous thread for bubble formation in a flow-focusing device: the neck collapses with a scaling exponent of 1/3 driven by a filling effect, followed by a liquid inertia driven stage, in which the collapse characterized by a scaling of 2/5. Lu *et al.* [28] observed also that the exponent is less than 1/3 in the beginning of the breakup and increases to 0.5 approaching to the final pinchoff, for the axisymmetric collapse of the gaseous thread for bubble formation in a flow-focusing device with cross-junctions. The exponent of 0.22 in the present experiment can be attributed to the squeezing of continuous phase and the asymmetric breakup of the bubbles at the T junction, as Gordillo *et al.* [30] insisted that the exponent for asymmetric breakup of the bubble is less than the axisymmetric breakup. The faster asymmetric collapse can be physically explained as follows: in the asymmetric breakup the gas velocity inside the neck increases approaching to the final pinchoff, resulting in a suction originated by the high-speed gas stream to accelerate the liquid toward the axis [30]. The exponent of 0.5 can be attributed to the breakup of the free gas-liquid surface and is consistent with the scaling law for the breakup of free gas-liquid surface in conventional bubbling device [31–33], in which the scaling law is the evidence for the bubble breakup under the combined action of the surface tension and the inertia

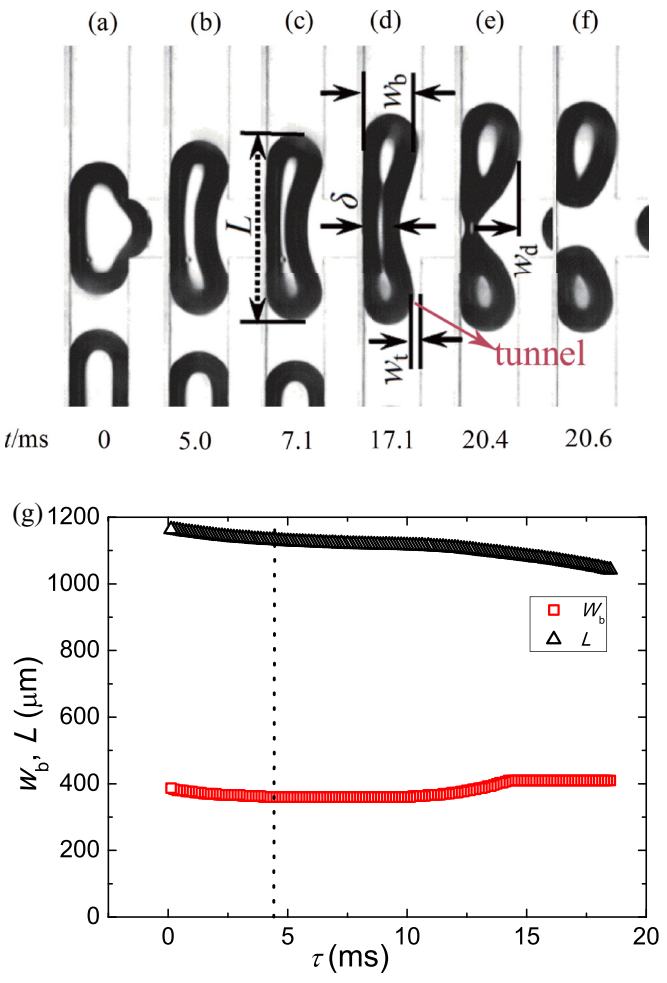

FIG. 9. (a)–(f) Bubble breakup in regime B; (g) evolution of the maximum width of the bubble tip w_b and length of the bubble L with the remaining time τ. $Q_l = 30$ mL/h, $Q_g = 15$ mL/h. The capillary number Ca = 0.004362. The vertical dotted line characterizes the critical remaining time between the fast- and slow-breakup stages. The width of tunnel between the bubble tip and the channel wall is designated as w_t.

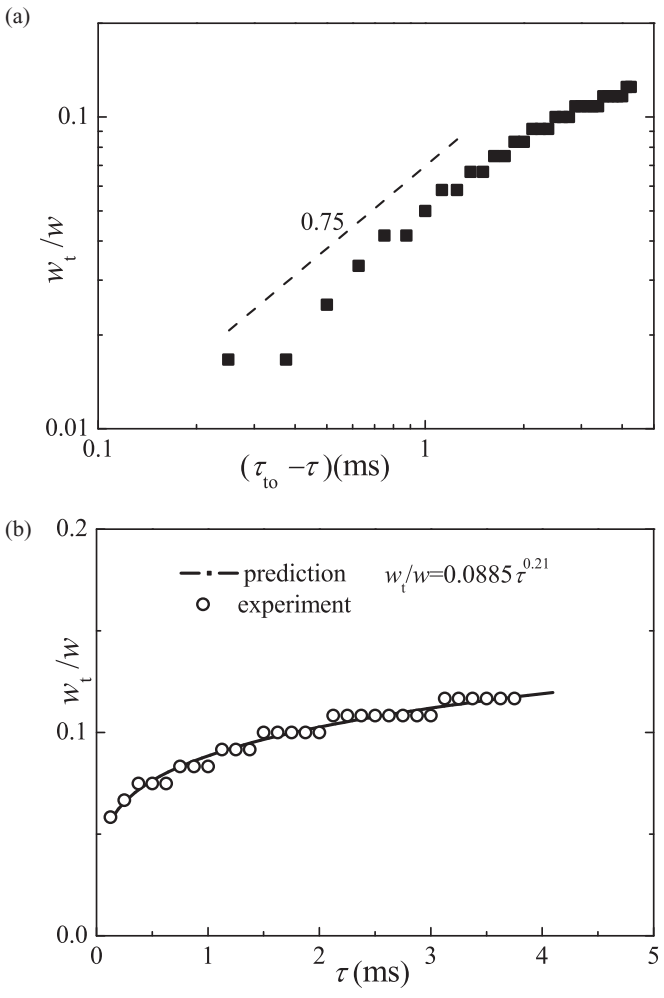

FIG. 10. Evolution of dimensionless tunnel width w_t/w during bubble breakup in regime B: (a) with the time $(\tau_{to} - \tau)$ in slow-breakup stage, $\delta > \delta_c$; (b) with the remaining time τ in the fast-breakup stage, $\delta < \delta_c$. τ_{to} is the remaining time at the onset of the opening of the tunnel between the bubble tip and the channel wall. $Q_l = 30$ mL/h, $Q_g = 15$ mL/h. The capillary number Ca = 0.004362.

of the continuous phase [27]. From Fig. 8, the critical width of the neck of the breakup bubble δ_c/w is found to be between 0.5 and 0.6.

It is noteworthy that the scaling law for the evolution of the long bubble breakup without tunnels at a T junction in the regime A in the present work is incompatible with the reported results for droplet breakup at T junctions [17] or breakup for bubble formation in flow-focusing devices [26–28]. An exponent of unity was observed for the evolution of the minimum width of the droplet neck with the time for droplet breakup in a T junction [17]. This deviation may be caused by the different flow systems. According to the report of Gordillo *et al.* [30], there is obvious divergence for the scaling law for the breakup of the droplet and bubble. Furthermore, Fu *et al.* [18] and Dollet *et al.* [26] observed a 1/3 scaling law for the breakup dynamics for bubble formation in a flow-focusing device, followed by a scaling law with the exponent of 2/5 or 1/2, depending on the geometry of the flow-focusing devices [27,28].

C. Mechanism and dynamics of bubble breakup at the T junction in flow regime B

The breakup of a bubble at the T junction in regime B can be categorized into three stages as shown in Fig. 9. At first, when a bubble enters the T junction, the bubble neck diminishes and the depression region extends under the squeezing of continuous phase. When the depression region extends to the bubble tip, the tip detaches from the channel wall on the incoming flow side to form a tunnel between the bubble and the channel wall, through which the continuous phase can leak. When the minimum width of the bubble neck diminishes to a critical value, the arc-shaped gas-liquid surface of the depression region shrinks suddenly, leading to the detachment of the bubble neck from the subjacent channel wall and the reduction of the width of the tunnel. After then, the bubble breaks up rapidly into two secondary daughter bubbles. The evolution of the maximum width of the bubble tip w_b and the length of the bubble L with the remaining time τ is shown in Fig. 9(g). In the slow breakup stage, the length of the bubble increases linearly and the slope before the appearance of the tunnel is larger than that after the appearance of the tunnel. In the fast-breakup stage, the length of the bubble increases nonlinearly.

In the slow-breakup stage, the maximum width of the bubble tip w_b decreases nonlinearly with time after the detachment of the tip from the channel wall until a minimum value and then it increases nonlinearly. Therefore, the width of the tunnel $w_t(w_t = w - w_b)$ increases with time after the detachment of the tip from the channel wall until a maximum value and then decreases with time. A power-law relationship is observed between the width of the tunnel and the time

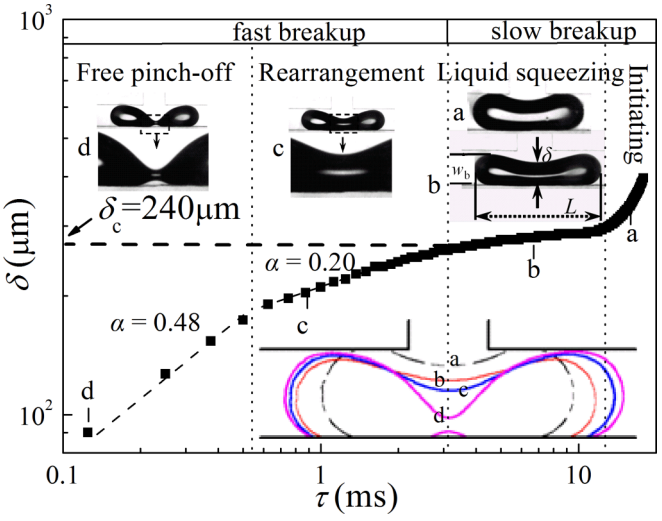

FIG. 11. Evolution of the minimum width of bubble neck with the remaining time in regime B. The insets (a)–(d) were the optical micrographs of the gas-liquid interface for the breaking bubble. The subjacent inset gives the evolution of bubble profile. $Q_l = 30$ mL/h, $Q_g = 15$ mL/h. The capillary number Ca = 0.004362. The vertical dotted lines differentiate the boundaries between adjacent stages. The horizontal dashed line represents the critical minimum width of the breaking bubble δ_c.

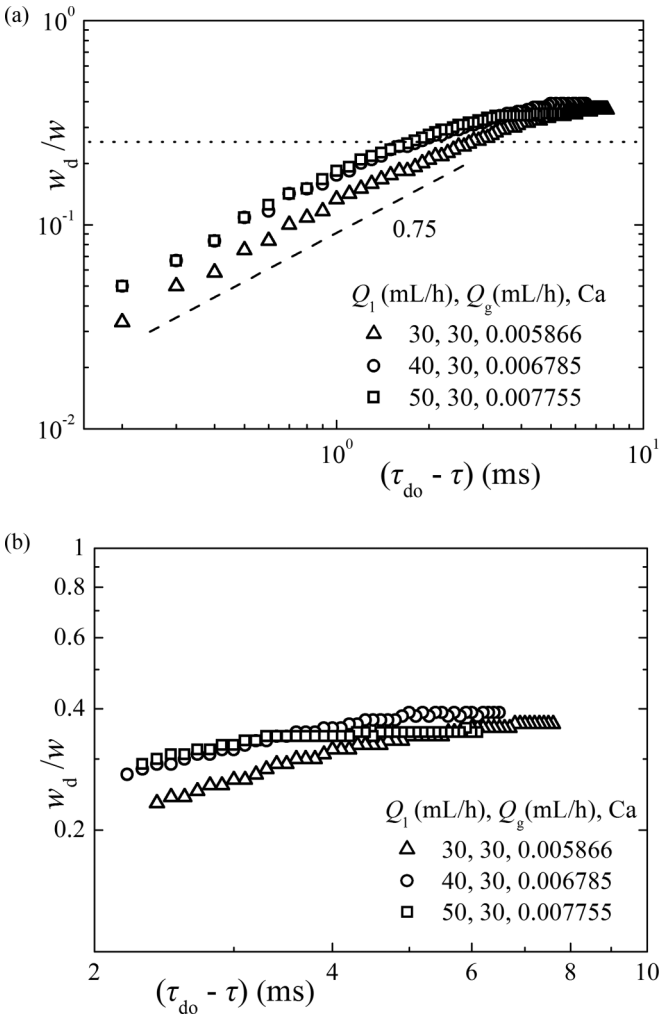

FIG. 12. Evolution of the dimensionless width of depression region w_d/w with the time $(\tau_{do} - \tau)$ during slow breakup in regime B: (a) before the tunnel was formed; (b) after the tunnel was formed. τ_{do} is the remaining time before the final pinchoff when the depression region starts to form. The horizontal line differentiates the slow- and fast-breakup stages.

$(\tau_{to} - \tau)$ with an exponent of 0.75, during the increment of the width of the tunnel as shown in Fig. 10(a). τ_{to} is the remaining time at the onset of the opening of the tunnel between the bubble tip and the channel wall. This scaling law is consistent with that for the evolution of the width of the depression region in the slow-breakup stage in flow regime A as shown in Fig. 7, signifying that the evolution of the tunnel is predominated by the squeezing of the liquid. However, the width of the tunnel decreases nonlinearly with time in the fast-breakup stage. A power-law function is observed between the width of the tunnel and the remaining time with an exponent of 0.21 as shown in Fig. 10(b): $w_t/w = 0.0885\tau^{0.21}$. This tendency is consistent with the result of the initial stage for the fast breakup in regime A, suggesting that the diminishing of the tunnel width is controlled by the combined action of the liquid squeezing and surface tension. The variation of the tunnel width during the bubble breakup at a T junction is also found in the work of Fu *et al.* [18].

The evolution of the minimum width of the bubble neck with the remaining time in regime B is illustrated in Fig. 11. The critical minimum width of the neck of the breaking bubble is found to be 0.6 in Fig. 11: $\delta_c/w = 240/400 = 0.6$. The thinning of the bubble neck experiences an initiating stage, a liquid-squeezing slow-breakup stage, followed by a fast-breakup stage. The fast-breakup stage includes the rearrangement stage and the free pinchoff stage, characterized by the different thinning rates in the two substages. The rearrangement stage is the intermediate status of the gas-liquid interface that locally relaxes interfacial energy induced either by the coarsening process or by an applied shear strain around the interface, which can be triggered by the squeezing of the liquid [34,35]. The tendency for the fast breakup in regime B is consistent with that in regime A, indicating that the presence of a tunnel in regime B does not influence the fast breakup. This can be understood by the fact that the fast pinchoff stage is driven by the liquid inertia and surface tension under the confinement, which is predominated by the local flow dynamics around the gas neck [27,29]. However, in the slow-breakup stage, there is obvious divergence for the evolution of the minimum width of the bubble neck before

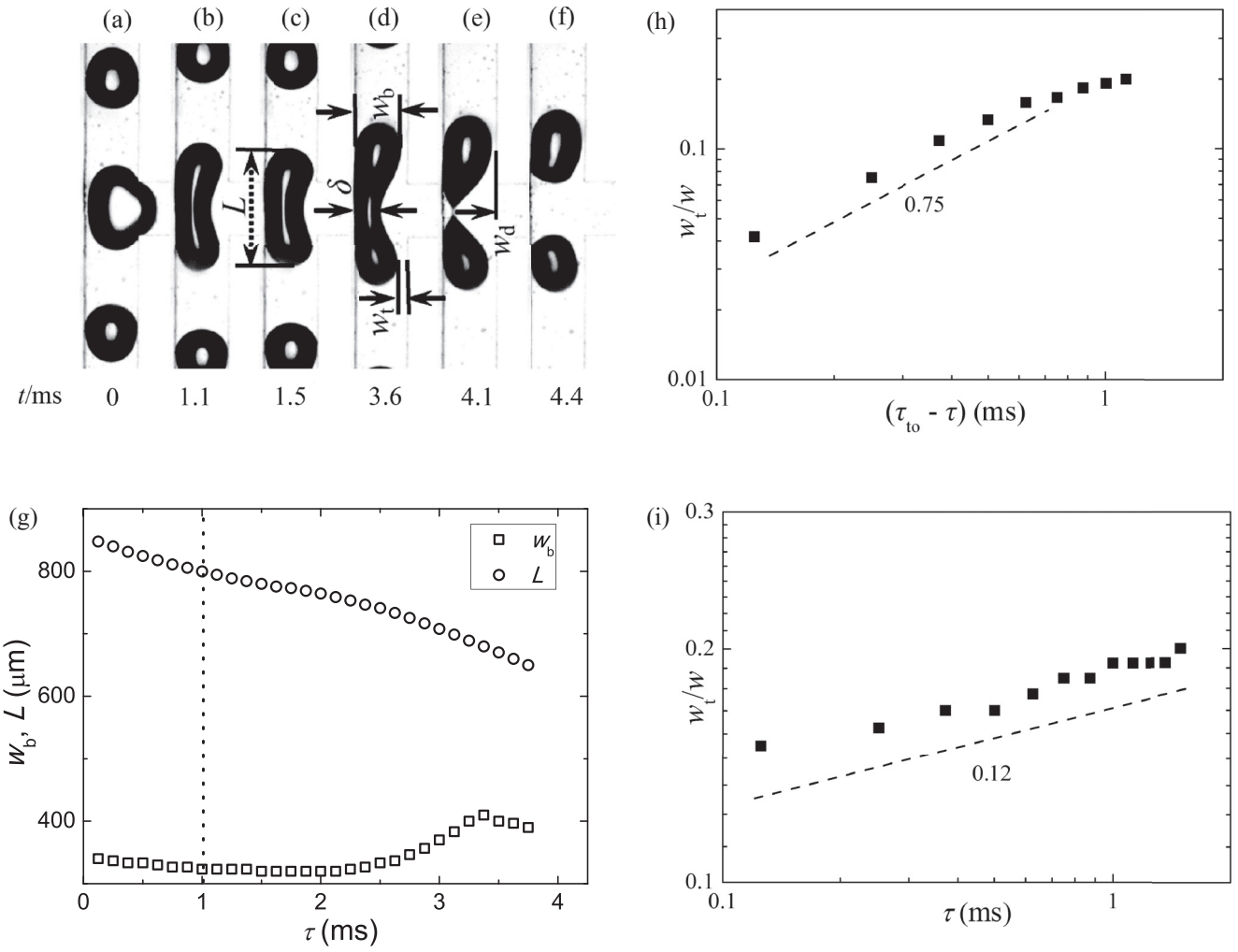

FIG. 13. (a)–(f) Bubble breakup in regime C. (g) Evolution of the maximum width of the bubble tip w_b and length of the bubble L with the remaining time τ. The vertical dotted line characterizes the critical remaining time between the fast- and slow-breakup stages. (h) Evolution of tunnel width with the time $(\tau_{to} - \tau)$ in slow breakup stage, τ_{to} is the remaining time at the onset of the opening of the tunnel between the bubble tip and the channel wall. (i) Evolution of tunnel width with the remaining time during fast breakup. $Q_l = 120$ mL/h, $Q_g = 40$ mL/h. The capillary number Ca = 0.01551.

and after the appearance of the tunnel. Therefore, we discuss the evolution of the minimum width of the bubble neck in the slow-breakup stage only. A power-law function is observed between the width of the depression region and the time $(\tau_{do} - \tau)$ before the appearance of the tunnel with an exponent of 0.75, as shown in Fig. 12(a). This tendency is consistent with the results in the slow breakup in regime A, suggesting that the breakup is driven by liquid squeezing before the appearance of the tunnel. However, after the opening of the tunnel, the rate of the breakup decreases rapidly and a logarithmic function is observed between the width of the depression region and the time $(\tau_{do} - \tau)$ as $w_d/w \propto a \ln(\tau_{do} - \tau) + b$, as shown in Fig. 12(b). The decrease of the breakup rate stems from the decrease of the pressure in the depression region with the widening of the tunnel. This is consistent with the work of Jullien *et al.* [15], in which, the different thinning rates of the droplet breakup before and after the appearance of the tunnel were also observed.

D. Mechanism and dynamics of bubble breakup at the T-junction in flow regime C

As shown in Figs. 13(a)–13(f), the bubble tip detaches the channel wall in the main channel direction as soon as the bubble enters the T junction. Then, the continuous phase can leak from the tunnel between the bubble and the channel wall to widen the tunnel and to thin the bubble neck. When the minimum width of the bubble neck diminishes to a critical value, the arc-shaped gas-liquid interface of the depression region contracts suddenly, and the neck detaches from the subjacent channel wall. The bubble breaks up rapidly into two secondary bubbles, with the diminishing of the width of the tunnel. The evolution of the maximum width of the bubble tip w_b and the length of the bubble L with the remaining time τ is shown in Fig. 13(g). The evolution of the length of the breaking bubble is consistent with that in regime B: the length of the bubble increases linearly in the slow-breakup stage, and increases nonlinearly in the fast-breakup stage [Fig. 13(g)]. Analogous to the regime B, the width of the tunnel follows a power-law function with the time in the slow-breakup stage with an exponent of 0.75, and it follows a power law with the remaining time in the fast-breakup stage with an exponent of 0.12 as shown in Figs. 13(h) and 13(i). It is worth noting that the evolution of the bubble length and the tunnel width in regime C are consistent with those in regime B, signifying that the deformation of the bubble is predominated by the liquid flow around the deforming bubble in the microchannel, for both the medium-sized bubble in regime B and the short bubble in regime C. However, the exponent 0.12 in regime C is almost half the value of 0.21 found in regime B, demonstrating that the evolution of the tunnel in the fast-breakup stage is also affected by the flow within the bubble that is associated with the bubble size, that's to say, the width of the bubble tip evolves at different rates in regimes B and C, which is predominated by the flow within the bubble that is induced by the fast contraction of the bubble neck by keeping the volume conservation of the bubble.

The evolution of the minimum width of the bubble neck with the remaining time in regime C is illustrated in Fig. 14. The thinning of the bubble neck experiences also an initiating

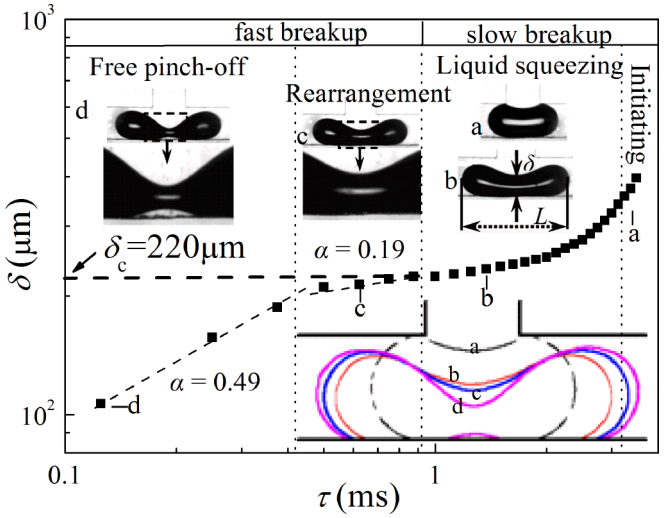

FIG. 14. Evolution of the minimum width of the bubble neck with the remaining time in regime C. The insets (a)–(d) were the optical micrographs of the gas-liquid interface for the breaking bubble. The subjacent insets give the evolution of the bubble profile. Q_l = 80 mL/h, Q_g = 40 mL/h. The capillary number Ca = 0.01163. The vertical lines differentiate the boundaries between adjacent stages. The horizontal dashed line represents the critical minimum width of the breaking bubble δ_c.

stage, a liquid-squeezing slow-breakup stage, followed by a fast-breakup stage. The fast-breakup stage includes the rearrangement stage and the free pinchoff stage, characterized by the different thinning rates in the two substages. The tendency of the fast breakup in regime C is consistent with that in the regime A. However, the tendency in the slow breakup in regime C deviates from that in the regime B. The critical width of the neck of the breakup bubble δ_c/w is found to be 0.55 in Fig. 14. As shown in Fig. 15, a logarithmic function is

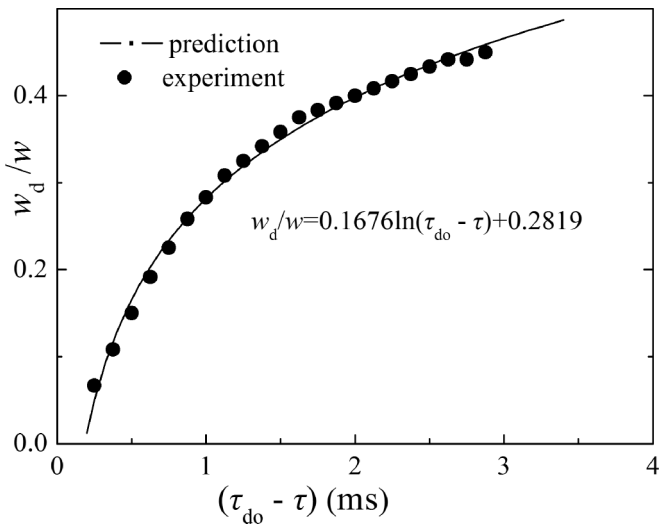

FIG. 15. Evolution of the dimensionless width of the depression region w_d/w with the time $(\tau_{do} - \tau)$ during the slow breakup of bubbles in regime C. τ_{do} is the remaining time before the final pinchoff when the depression region starts to form. Q_l = 80 mL/h, Q_g = 40 mL/h. The capillary number Ca = 0.01163.

observed between the width of the depression region and the time ($\tau_{do} - \tau$) and the rate of the breakup decreases rapidly with time, as the pressure in the depression region diminishes rapidly with the augmented leaking of the continuous phase through the tunnel.

IV. CONCLUSIONS

To conclude, the evolution of the gas-liquid interface during the breakup of bubbles at a T junction under the confinement of microchannels was investigated as shown in Table II. Four regimes were observed for bubbles flowing through the T junction. It was identified by the stop flow that a critical width of the bubble neck existed: if the minimum width of the bubble neck was less than the critical value, the breakup was irreversible; otherwise, the breakup was reversible. The critical minimum width of the bubble neck differentiating the fast- and slow-breakup stages is found to be 0.5–0.6 in the present study as shown in Table I. This value is quite close to the predicted value of 0.5 either for the onset of the breakup of a droplet in Leshansky *et al.* [14] or for the onset of the rapid breakup of a droplet in Hoang *et al.* [17]. For the fast-breakup process, the minimum width of the bubble neck could be scaled with the remaining time by a power law with an exponent of 0.22 in the beginning, and of 0.5 approaching the final pinchoff for the fast breakup of bubbles. These results suggested that the fast breakup of bubbles seemed to be driven by the surface tension and liquid inertia, according to that reported in Ref. [27], which was independent of the operating conditions. The slow breakup was driven by the continuous phase and depends on the type of bubble breakup, owing to the complex geometrical variation of gas-liquid interface under the confinement at the junction. Before the appearance of the tunnel, the width of the depression region could be scaled with the time by a power law with an exponent of 0.75; while after that, the relationship between the width of the depression region and the time could be expressed as a logarithmic function. This work paves the way for further theoretical and numerical studies on interfacial dynamics for multiphase flow within high-viscosity and non-Newtonian fluids under confinement in complex microchannels, to better serve for the design and parallelization of microfluidic devices.

ACKNOWLEDGMENTS

The financial support for this project from the National Natural Science Foundation of China (Grants No. 21276175, No. 21576186, No. 91434204, and No. 21106093), the Tianjin Natural Science Foundation (Grant No. 13JCQNJC05500), the aid of Opening Project of State Key Laboratory of Chemical Engineering (Grant No. SKL-ChE-13T04), and the Program of Introducing Talents of Discipline to Universities (Grant No. B06006) are gratefully acknowledged.

[1] X. Wang, C. Zhu, T. Fu, and Y. Ma, Chem. Eng. Sci. **111**, 244 (2014).
[2] A. M. Gañán-Calvo, J. M. Montanero, L. Martín-Banderas, and M. Flores-Mosquera, Adv. Drug Deliv. Rev. **65**, 1447 (2013).
[3] W. Wang, M.-J. Zhang, R. Xie, X.-J. Ju, C. Yang, C.-L. Mou, D. A. Weitz, and L.-Y. Chu, Angew. Chem., Int. Ed. **52**, 8084 (2013).
[4] J.-T. Wang, J. Wang, and J.-J. Han, Small **7**, 1728 (2011).
[5] W. Li, K. Liu, R. Simms, J. Greener, D. Jagadeesan, S. Pinto, A. Günther, and E. Kumacheva, J. Am. Chem. Soc. **134**, 3127 (2011).
[6] J. Atencia and D. J. Beebe, Nature **437**, 648 (2005).
[7] A. Huerre, V. Miralles, and M.-C. Jullien, Soft Matter **10**, 6888 (2014).
[8] Y. Zhao, G. Chen, C. Ye, and Q. Yuan, Chem. Eng. Sci. **87**, 122 (2013).
[9] D. R. Link, S. L. Anna, D. A. Weitz, and H. A. Stone, Phys. Rev. Lett. **92**, 054503 (2004).
[10] P. Garstecki, M. J. Fuerstman, H. A. Stone, and G. M. Whitesides, Lab on a Chip **6**, 437 (2006).
[11] M. Al-Rawashdeh, X. Nijhuis, E. V. Rebrov, V. Hessel, and J. C. Schouten, AIChE J. **58**, 3482 (2012).
[12] L. Menetrier-Deremble and P. Tabeling, Phys. Rev. E **74**, 035303 (2006).
[13] M. Samie, A. Salari, and M. B. Shafii, Phys. Rev. E **87**, 053003 (2013).
[14] A. M. Leshansky and L. M. Pismen, Phys. Fluids **21**, 023303 (2009).
[15] M. C. Jullien, M. J. Tsang Mui Ching, C. Cohen, L. Menetrier, and P. Tabeling, Phys. Fluids **21**, 072001 (2009).
[16] A. M. Leshansky, S. Afkhami, M. C. Jullien, and P. Tabeling, Phys. Rev. Lett. **108**, 264502 (2012).
[17] D. A. Hoang, L. M. Portela, C. R. Kleijn, M. T. Kreutzer, and V. van Steijn, J. Fluid Mech. **717**, R4 (2013).
[18] T. Fu, Y. Ma, D. Funfschilling, and H. Z. Li, Chem. Eng. Sci. **66**, 4184 (2011).
[19] T. Fu, Y. Ma, and H. Z. Li, AIChE J. **60**, 1920 (2014).
[20] X. Wang, C. Zhu, T. Fu, and Y. Ma, AIChE J. **61**, 1081 (2015).
[21] X. Wang, C. Zhu, Y. Wu, T. Fu, and Y. Ma, Chem. Eng. Sci. **132**, 128 (2015).
[22] T. Fu and Y. Ma, Chem. Eng. Sci. **135**, 343 (2015).
[23] V. van Steijn, C. R. Kleijn, and M. T. Kreutzer, Phys. Rev. Lett. **103**, 214501 (2009).
[24] H. A. Stone, B. J. Bentley, and L. G. Leal, J. Fluid Mech. **173**, 131 (1986).
[25] P. Garstecki, H. A. Stone, and G. M. Whitesides, Phys. Rev. Lett. **94**, 164501 (2005).
[26] B. Dollet, W. van Hoeve, J.-P. Raven, P. Marmottant, and M. Versluis, Phys. Rev. Lett. **100**, 034504 (2008).
[27] W. van Hoeve, B. Dollet, M. Versluis, and D. Lohse, Phys. Fluids **23**, 092001 (2011).
[28] Y. Lu, T. Fu, C. Zhu, Y. Ma, and H. Li, Microfluid. Nanofluid. **16**, 1047 (2014).
[29] J. Eggers, M. A. Fontelos, D. Leppinen, and J. H. Snoeijer, Phys. Rev. Lett. **98**, 094502 (2007).

[30] J. M. Gordillo, A. Sevilla, J. Rodriguez-Rodriguez, and C. Martinez-Bazan, Phys. Rev. Lett. **95**, 194501 (2005).
[31] S. T. Thoroddsen, T. G. Etoh, and K. Takehara, Phys. Fluids **19**, 042101 (2007).
[32] J. Eggers and E. Villermaux, Rep. Prog. Phys. **71**, 036601 (2008).
[33] J. C. Burton, R. Waldrep, and P. Taborek, Phys. Rev. Lett. **94**, 184502 (2005).
[34] S. Cohen-Addad, R. Höhler, and O. Pitois, Annu. Rev. Fluid Mech. **45**, 241 (2013).
[35] J. H. Snoeijer and B. Andreotti, Annu. Rev. Fluid Mech. **45**, 269 (2013).